

# Evidence of type-I and type-II superconductivity and their coexistence in $\text{ZrB}_{12}$

P. K. Biswas,<sup>1,\*</sup> A. D. Hillier,<sup>1</sup> R. P. Singh,<sup>2</sup> N. Parzyk,<sup>3</sup> G. Balakrishnan,<sup>3</sup>  
M. R. Lees,<sup>3</sup> C. D. Dewhurst,<sup>4</sup> E. Morenzoni,<sup>5,†</sup> and D. M<sup>c</sup>K. Paul<sup>3</sup>

<sup>1</sup>*ISIS Pulsed Neutron and Muon Source, STFC Rutherford Appleton Laboratory,  
Harwell Campus, Didcot, Oxfordshire, OX11 0QX, United Kingdom*

<sup>2</sup>*Indian Institute of Science Education and Research Bhopal, Bhopal, 462066, India*

<sup>3</sup>*Physics Department, University of Warwick, Coventry, CV4 7AL, United Kingdom*

<sup>4</sup>*Institut Laue Langevin, 6 Rue Jules Horowitz, 38042 Grenoble, France*

<sup>5</sup>*Laboratory for Muon Spin Spectroscopy, Paul Scherrer Institut, CH-5232 Villigen PSI, Switzerland*

(Dated: April 28, 2022)

Superconductors are categorised as either type-I or type-II depending on their behaviour under a magnetic field. The existence of both types of superconductivity in the same material is rare and of great experimental and theoretical interest. Here we have used the muon spin rotation ( $\mu\text{SR}$ ) technique to unveil the superconducting phase diagram of the dodecaboride  $\text{ZrB}_{12}$ . Analysing the local magnetic field distribution obtained from the  $\mu\text{SR}$  spectra we identify regions of a Meissner state where the applied magnetic field is entirely expelled from the sample, an intermediate state where normal and Meissner states coexist, and a mixed state where a well-defined flux-line lattice is formed. Neutron diffraction data confirm the presence of a mixed state with a square flux-line lattice at all temperatures and applied magnetic above 175 Oe. While Meissner and intermediate states are the characteristic features of type-I superconductors, the mixed state exists only in type-II superconductors. We also observe regions of the phase diagram where the type-I and type-II states overlap and coexist, which is of relevance in the context of type-1.5 superconductivity. The results strongly suggest that the Ginzburg-Landau parameter of  $\text{ZrB}_{12}$  varies as a function of temperature so that pure type-I and type-II, as well as different coexisting states, are realised in this system.

PACS numbers:

The response of a superconductor in a magnetic field is characterised by distinct length scales, which depend on a few key parameters of the material [1]. The penetration depth,  $\lambda$ , describes the length scale of magnetic field variation. The coherence length,  $\xi$ , defines the length scale of the spatial variation of the macroscopic wave function describing the superconducting state. The ratio of these two quantities is the Ginzburg-Landau parameter,  $\kappa = \frac{\lambda}{\xi}$ . If  $\kappa < \frac{1}{\sqrt{2}}$ , the magnetic field is expelled or excluded from the body of a superconductor except for a layer of thickness  $\lambda$ . Such a superconductor is described as a type-I or soft superconductor. This property exists up to a critical field of  $H_c$ . For higher applied fields,  $H \geq H_c$ , the superconductor returns to the normal state and the field penetrates the bulk of the sample. The flux expulsion is known as the Meissner effect, and the superconductor behaves as an ideal diamagnet below  $H_c$ . However, in a sample with non-zero demagnetization factor ( $N > 0$ ) even in a small applied field fulfilling the condition  $H_c(T); (1 - N) \leq H \leq H_c(T)$ . The field along the surface can exceed the critical field in parts of the sample, especially at edges, thus allowing the magnetic flux to penetrate at these areas. In this situation, flux-free superconducting regions ( $B = 0$ ) and normal regions with an internal field of  $\approx B_c$  coexist microscopically and rather complex field textures are formed to minimise the total free energy. Such a state is known as the intermediate state and is a characteristic feature of a type-I superconductor. For superconductors with  $\kappa > \frac{1}{\sqrt{2}}$ , it

is energetically favourable for the magnetic flux to penetrate the sample in the form of flux-lines parallel to the applied field also known as Abrikosov vortices. The repulsive interactions between these vortices tend to produce a stable lattice structure (usually triangular) over the entire volume of a sample. These vortices exist from a lower critical field  $H_{c1}$  up to an upper critical field of  $H_{c2}$ . This state is called mixed state and is the main feature of a type-II superconductor. For  $H \geq H_{c2}$ , the vortices disappear due to the overlap of the core regions and the sample returns to the normal state. The interaction potential between vortex lines is attractive for Type-I and repulsive for Type-II systems, or equivalently the surface free energy between normal and Meissner domains positive and negative. An interesting situation arises around the point  $\kappa = \frac{1}{\sqrt{2}}$  where the interaction vanishes at all distances [2] or when the usually repulsive interaction in a type-II superconductor has an attractive tail. In this case both type-I and type-II behavior with regions in the Meissner state and regions filled with vortices have been observed in the same sample and named intermediate mixed state (IMS) [3–5]. More recently, the existence of a new type of superconducting state has been claimed in multi-band superconductors (‘type-1.5 superconductivity’ in  $\text{MgB}_2$ ) based on similar observations [6, 7]. Experimentally such coexisting states have been generally visualized by decoration and SQUID scanning techniques or inferred from magnetization measurements.

Superconductivity in  $\text{ZrB}_{12}$  was first observed by

Matthias *et al.* [8, 9] in the late 1960's. Amongst the dodecaborides  $MeB_{12}$  ( $Me = Sc, Y, Zr, La, Lu, Th$ )  $ZrB_{12}$  has a relatively high  $T_c$  of 6.1 K and displays a variety of deviations from the conventional superconducting behaviour. Several models have been proposed to explain its superconducting properties, including the picture of  $ZrB_{12}$  as a conventional superconductor with enhanced surface effects [10, 11], as a strongly-coupled  $s$ -wave material [12], or as a superconductor with different superconducting gaps and  $T_c$ 's described by a two-band Bardeen-Cooper-Schrieffer (BCS) model [13]. Even  $d$ -wave superconductivity has been proposed for this compound [14]. These arguments continue to this day [17]. Recent band-structure calculations concluded that the Fermi surface of  $ZrB_{12}$  is composed of an open and a closed sheet [18] which might be the source of multi-band character. The value of  $\kappa$  is close to  $\frac{1}{\sqrt{2}}$  so that this material lies very close to the cross-over region between type-I and type-II superconductivity [10]. Specific heat measurements as a function of field show a normal-to superconducting-state transition which changes from a first-order type with latent heat, to a second-order type without latent heat with increasing magnetic field [19].

Here we report muon spin rotation/relaxation ( $\mu$ SR) measurements on single crystals of  $ZrB_{12}$ . This technique has been widely used to map the phase diagram and study the microscopic properties of the vortex and Meissner state of superconductors [20, 21]. Investigations of the intermediate state by  $\mu$ SR have been limited to a few elemental superconductors [22–25], however, recently, there has been increased attention in conjunction with the nature of the superconductivity of the noncentrosymmetric BeAu [26, 27]. We mapped the inhomogeneous magnetic field distributions and identify and characterise the different superconducting states in the  $H$ - $T$  phase diagram of  $ZrB_{12}$ , which includes, beside Meissner, mixed and intermediate state, a mixed-Meissner state and a mixed-intermediate state. To our knowledge the latter has never been observed previously. We ascribe this behavior to a temperature dependent  $\kappa$  parameter. This result suggests that in a material with low, temperature dependent  $\kappa$  the full richness of superconducting states can be realized and can coexist.

The  $\mu$ SR experiments were carried out using the MuSR spectrometer [28] of the ISIS facility at the Rutherford Appleton Laboratory. A mosaic of seven single crystal discs of  $ZrB_{12}$  (of thickness 1.5-2 mm, and diameter 4-5 mm), all aligned with the crystallographic  $c$ -axis parallel to the incident muon beam, was used for the experiment. The measurements were performed in the transverse-field (TF) configuration, i.e. with the magnetic field applied perpendicular to the initial muon spin polarisation. In the chosen geometry the demagnetisation factor of the samples is between 0.24 and 0.3. We applied fields between 50 and 600 Oe to fully cover the superconducting phase diagram of  $ZrB_{12}$  and field cooled the sample.

The TF- $\mu$ SR asymmetry spectra were transformed into a probability of field versus magnetic field spectra by a Maximum Entropy (MaxEnt) algorithm [29] to identify the dominant field components. Based on this information, the TF- $\mu$ SR spectra were analysed in the time domain using a sum of Gaussian field distributions to quantify the different magnetic field distributions present in the sample as a function of temperature and field. Details of the  $\mu$ SR technique, of the sample preparation and characterisation, and of the fitting functions are given in the Supplemental Material.

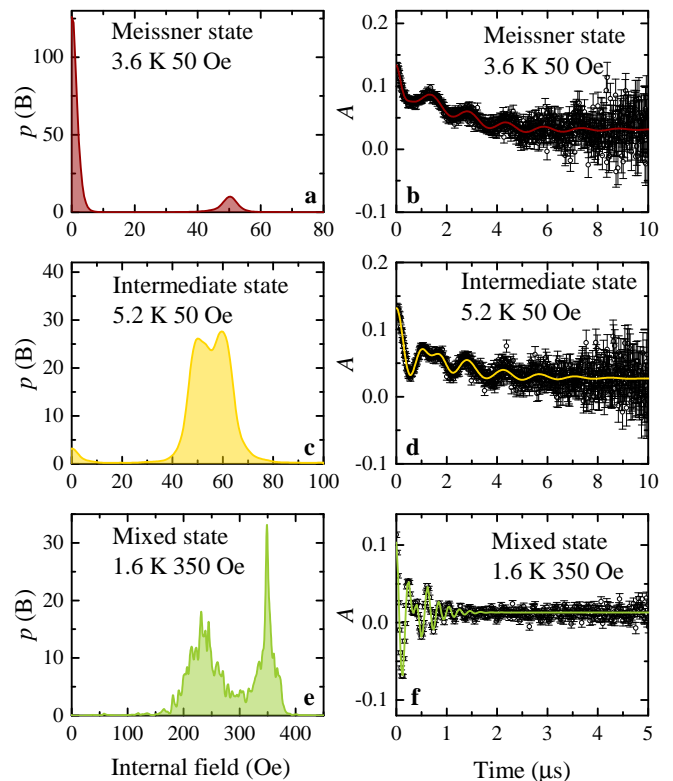


FIG. 1: Field distribution,  $p(B)$ , of the local field probed by muons obtained by MaxEnt transformation of the TF- $\mu$ SR time spectra at different temperatures and applied fields. The figure illustrates the typical signal observed in the **a** Meissner, **c** intermediate, and **e** mixed states. **b**, **d**, and **f** show the TF- $\mu$ SR time spectra for the corresponding states. The solid lines are fits to the data using the function described in the Supplemental Material.

Figure 1 shows some typical MaxEnt analysis of the raw TF- $\mu$ SR time spectra for the magnetic field distribution in the **a** Meissner, **c** intermediate and **e** mixed states. Figures 1 **b**, **d**, and **f** show the TF- $\mu$ SR time spectra for the corresponding states. The solid lines are the fits to the data. Details of the fit function are given in the Supplemental Material. At 3.6 K, for an applied field of 50 Oe, which is well below  $H_{c1}$  at this temperature,  $ZrB_{12}$  is in the Meissner state. This is clearly reflected in the observed field distribution showing a strong component at

zero magnetic field. The presence of Zr nuclear moments leads to a typical slow relaxation of a Kubo-Toyabe type [30] for the zero field component. The weak contribution at the applied field value is a background signal that is mainly due to the muons stopping in the cryostat walls and other parts of the sample holder. The absence of any additional peaks implies that the magnetic field is completely expelled from the body of the superconductor. In a type-I superconductor, demagnetisation effects may induce the intermediate state, a stable coexistence of the magnetic fields with regions of zero field and regions of internal field  $\approx B_c$ . The topology of these regions can be fairly intricate and depends on several factors, such as sample shape and magnetic history. Existence of the intermediate state in ZrB<sub>12</sub> is clearly seen in the MaxEnt data and the corresponding time spectra, collected at 5.2 K and 50 Oe (see Fig. 1 c). Besides the background peak at 50 Oe, we also observe a peak at higher field  $\approx 60$  Oe, as well as a peak at  $B = 0$ , as expected in the intermediate state. In an applied field of 350 Oe (between  $H_{c1}$  and  $H_{c2}$ ), ZrB<sub>12</sub> is found in the mixed state. Such a state is characterised by the presence of a lattice of quantized flux lines. This leads to a distribution of internal fields starting at a minimum value and increasing in weight up to the so-called saddle point of the field distribution, which is the most probable field, before falling with a long tail to a maximum field value corresponding to the region close to the vortex core. This signal is well described by a Gaussian distribution of fields centred at the saddle point, which is around 230 G in this case, (see Fig. 1 e), and displays the expected diamagnetic shift with respect to the applied field. Also in this case we observe a background signal at the applied field of 350 Oe. It is important to note that the absence of the peak at  $B = 0$  shows that the full volume of the sample is in the mixed state.

In Fig. 2, the time-dependent asymmetry spectra (b and d) and the corresponding MaxEnt visualisation (a and c) clearly demonstrate that there are regions with inhomogeneous field distribution in the phase diagram displaying a coexistence of the Meissner and the mixed states as well as a coexistence of the intermediate and the mixed state. We denote these regions as the mixed-Meissner and mixed-intermediate states, respectively. Figures 2 e and f show that at 1.4 K, for an applied field of 500 Oe, ZrB<sub>12</sub> returns in the normal state. Here, the field penetrates the bulk of the sample completely, and we observe a homogeneous field distribution in the TF- $\mu$ SR time spectra, corresponding to a single peak at the applied field position in the MaxEnt data.

Figures 3 a, b, and c show the MaxEnt visualisation of the local field distribution as a function of temperature, collected for three different applied fields. Figure 3 a shows the temperature dependence of the internal field distribution at 50 Oe, displaying the change from Meissner to intermediate to normal state with increasing tem-

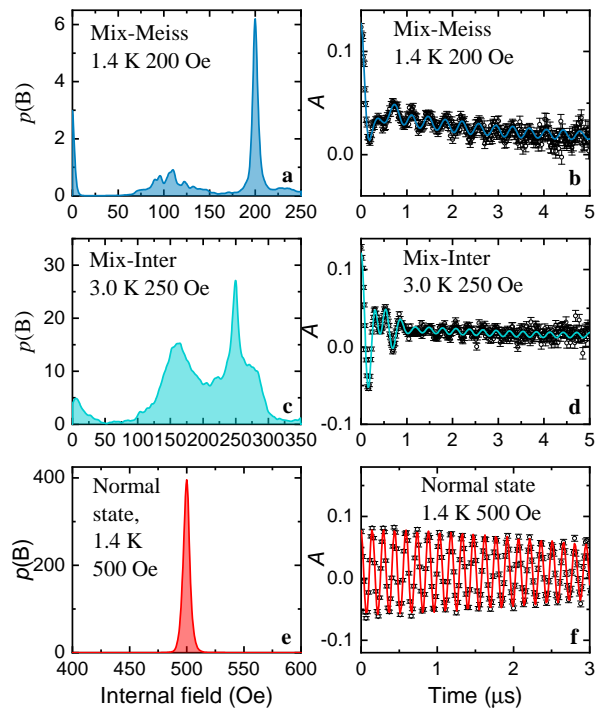


FIG. 2: Field distribution,  $p(B)$ , of the local field probed by muons and obtained by MaxEnt transformations at different temperatures and applied fields. The figure illustrates the typical signals observed in the **a** Mix-Meiss, **c** Mix-Inter, indicating the coexistence of type-I and type-II behaviour and **e** normal states. **b**, **d**, and **f** show the TF- $\mu$ SR time spectra for the corresponding states. The solid lines are fits to the data using the function described in the Supplemental Material.

perature. Similarly, figures 3 b and c exhibit an evolution from the mixed-Meissner to the mixed-intermediate to the normal state at 200 Oe and from the mixed to the normal state at 350 Oe, respectively. The variation of the local field distribution at different magnetic fields and temperatures clearly demonstrate that it is possible to drive the system into various superconducting states with the help of external parameters, such as field and temperature.

TF- $\mu$ SR data collected at various fields and temperature are summarised in a  $H$ - $T$  phase diagram in Fig. 4 a. A distinctive feature of the phase diagram is the existence of three separate superconducting phases, namely the Meissner, mixed, and intermediate states, as well as the appearance of mixed-Meissner and mixed-intermediate regions where two phases of different type coexist. A coexistence of mixed and Meissner state at the boundary of the two phases has been revealed from decoration

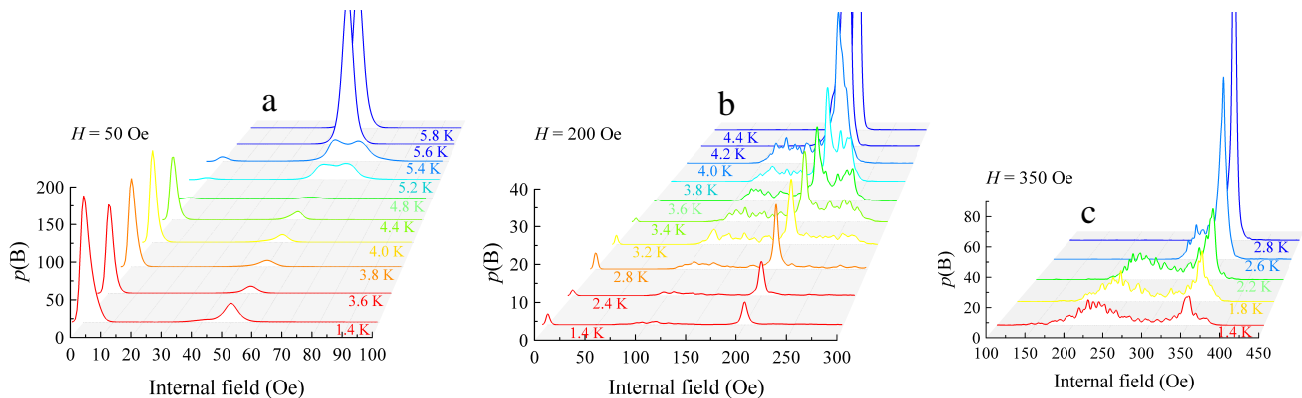


FIG. 3: Local field distribution probed by the muons,  $p(B)$ , obtained by MaxEnt transformation of the TF- $\mu$ SR time spectra collected at different temperatures and applied fields. The figure illustrates the change from **a** Meissner to intermediate to normal state at 50 Oe, **b** Mix-Meiss to Mix-Inter to normal state at 200 Oe, and **c** mixed to normal state at 350 Oe.

experiments and computations for superconductors with  $\kappa$  close to  $\frac{1}{\sqrt{2}}$  [4, 5] and for elemental Nb by small angle neutron scattering experiments [15, 16].

One condition for this state (also named intermediate mixed state, IMS) to occur is that besides the usual repulsive interaction within the vortices, it also has an attractive component [31]. A close experimental situation featuring both type-I and type-II behaviour was found in a multi-band superconductor such as  $\text{MgB}_2$  [6, 32], which shows regions with an inhomogeneous clustering of vortices and regions void of vortices. It was argued that the different coherence lengths and penetration depths of the two bands of  $\text{MgB}_2$  place the superconductor in a regime of a unique combination of a type-I and type-II superconductor realizing a novel superconducting state named ‘type-1.5 superconductivity’, fundamentally different from type-I and II. This behaviour, consistent with a theoretical modelling of the semi-Meissner state of a two-component superconductor [7], was also related to an attractive intervortex interaction. Usually, in a type-II superconductor, such interactions are primarily repulsive. However, at low fields where the flux-lines are separated by a considerable distance, there may be a small attractive component.

Further theoretical work on this topic has predicted that a type-1.5 behaviour can also arise in the case where only one band is truly superconducting while superconductivity in the other band is induced by an inter-band proximity effect [33]. The idea of ‘type-1.5 superconductivity’ was, however, later rejected by E. H. Brandt *et al.* who remarked that the assumption of two independent order parameters with different penetration depths and coherence lengths is unphysical for a superconductor with single transition temperature  $T_c$  [31]. K. V. Grigorishin has also suggested that such a scenario would violate the phase relations between the order parameters [34]. Experimentally, such a state is also difficult to distinguish

from a mixture of a vortex state with disorder induced by pinning at low fields and a Meissner state. Our experimental finding on  $\text{ZrB}_{12}$  showing the realization of a wide and rich coexistence region in a low-kappa type-II superconductor is of relevance in this context suggesting that it may not be necessary to postulate a new superconducting type to explain the observation.

We have also determined the temperature dependence of the GL parameter  $\kappa$  (see Fig. 4 b) using the expression  $\kappa = \frac{H_{c2}}{\sqrt{2}H_c}$  where  $H_c$  is the thermodynamic critical field and  $H_{c2}$  is defined here as the field of flux entrance. The temperature dependence of  $H_c$  and  $H_{c2}$  were estimated from the virgin magnetisation curves of  $\text{ZrB}_{12}$ , shown in the Supplemental Material. The value of  $\kappa$  is found to be very close to  $\frac{1}{\sqrt{2}}$  for  $T \gtrsim 4$  K thus confirming type-I superconductivity in  $\text{ZrB}_{12}$ .  $\kappa$  increases as we lower the temperature: at 1.8 K it is clear that the material is well into the type-II region. The temperature evolution of  $\kappa(T)$  is in agreement with the microscopic  $\mu$ SR results and demonstrates that the change with temperature produces both type-I and type-II superconductivity and the corresponding coexistence phases in the same material.

Small-angle neutron scattering (SANS) measurements allow us to confirm and characterise the flux-line lattice (FLL) in the mixed state of  $\text{ZrB}_{12}$ . The measurements were done using a different crystal to those used for the  $\mu$ SR measurements as we had to replace natural B with  $^{11}\text{B}$  isotope to reduce the neutron absorption. The measurements were performed using the D22 instrument at ILL, Grenoble. Further details of the SANS technique are given in the Supplemental Material. An example of the diffraction images obtained is presented in Fig. 5 for an applied field along the  $a$  axis. It is interesting to note that the flux-line lattice is square for all fields and temperatures in the mixed state of  $\text{ZrB}_{12}$ . Non-hexagonal vortex lattices are often associated with unconventional superconductivity [35]. However, such effects can also be

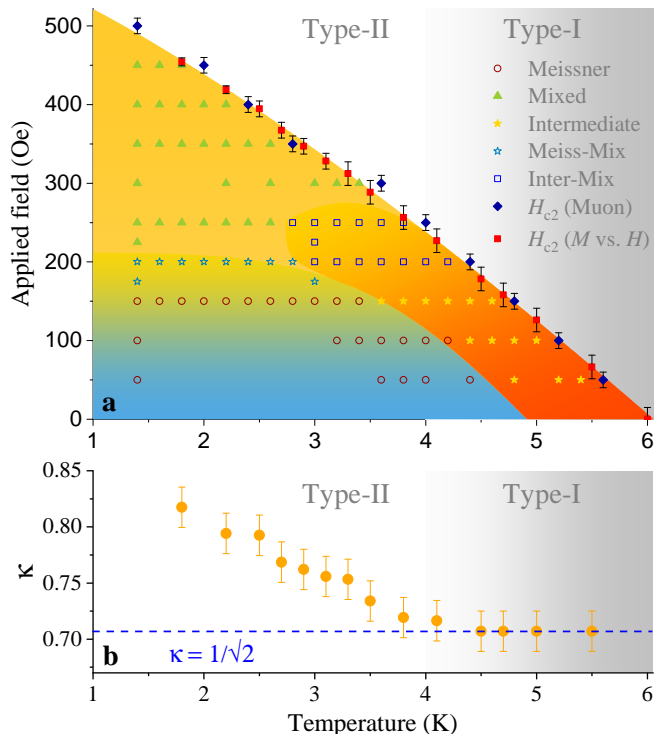


FIG. 4: **a** Different superconducting phases of  $\text{ZrB}_{12}$  as described in the text. The majority of the data come directly from the muon measurements. Also included are magnetisation measurements of  $H_{c2}$ . The points in the  $H$ - $T$  plane indicate where the data were obtained after field cooling and their colours show the assignment drawn from the MaxEnt analysis of the internal field distribution. The phase boundaries were determined by fitting the TF- $\mu$ SR time spectra to the expression described in the Supplemental Material. **b** Temperature dependence of the GL parameter  $\kappa$ , estimated from the  $H_c(T)$  and  $H_{c2}(T)$  as described in the text.

produced by non-locality [36, 37]. Since our experimental data suggest that  $\text{ZrB}_{12}$  is a marginal superconductor with a large core, it is likely that for an applied field along a high symmetry cubic direction, the super-currents flow around the core will also have square symmetry and the associated flux-line lattice will also be square.

To conclude, by  $\mu$ SR and neutron measurements we have elucidated a rich superconducting phase diagram of  $\text{ZrB}_{12}$ . This works decisively demonstrates that in a marginal superconductor such as  $\text{ZrB}_{12}$ , a change of temperature can produce both type-I and type-II characteristics in the same compound. The evolution of the two types is related to a gradual change of kappa with temperature. The mixed state is stable at all temperatures when the applied magnetic field is greater than 275 Oe up to  $H_{c2}$ . It would be interesting to extend our studies using low energy muon beams [21] to probe the near surface region in order to map and compare the superconductivity in this region with the bulk and to address the role of multi-band effects on surface superconductivity. It would

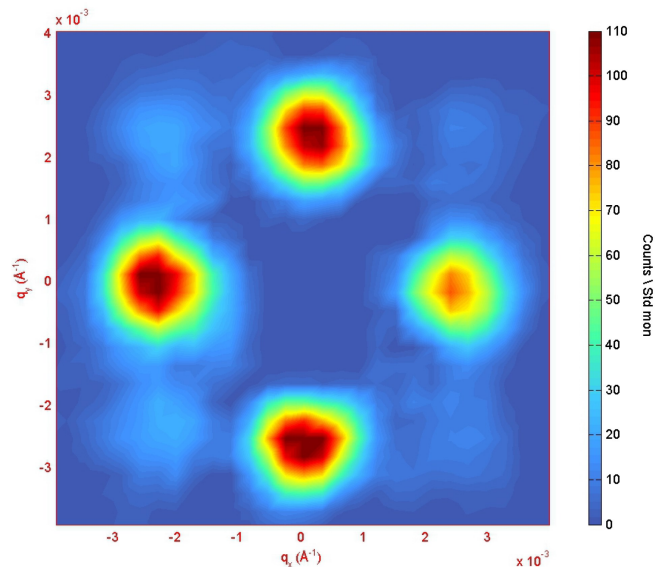


FIG. 5: Neutron diffraction image of the scattered intensity from the flux-line lattice in  $\text{ZrB}_{12}$ . The lattice was grown under an applied field of 300 Oe and the measurement performed at 1.6 K using a neutron wavelength of 10 Å. This figure was produced by counting with the neutron beam approximately parallel to the applied magnetic field. The presence of higher order reflections in this image indicates that a rather well ordered lattice structure is produced by the cooling procedure.

be also interesting to study such  $H$ - $T$  phase diagram in other low- $\kappa$  superconductors to verify its universality.

The  $\mu$ SR experiments were performed at the ISIS Pulsed Neutron and Muon Source, STFC Rutherford Appleton Laboratory, Didcot, United Kingdom. The small angle neutron diffraction experiments were performed at the Institut Laue Langevin, Grenoble, France. This work was supported by the Engineering and Physical Sciences Research Council (EPSRC) at Warwick through Grant No. EP/I007210/1 and the Science and Technology Facilities Council (STFC) of the UK. P.K.B would like to thank the Midlands Physics Alliance Graduate School (MPAGS) for financial support. We also wish to acknowledge useful comments from Professor Vladimir Kogan of Ames Laboratory.

\* pabitra.biswas@stfc.ac.uk

† Electronic address: elvezio.morenzoni@psi.ch

- [1] Tinkham, M. Introduction to Superconductivity. *2nd ed.* (Dover Publications, 2004).
- [2] Brandt, E. H., *Phys. Rev. B* **34**, 6514 (1986).
- [3] Krägeloh, U. *Phys. Lett.* **28A**, 657 (1969).
- [4] Krägeloh, U. Der Zwischenzustand bei Supraleitern zweiter Art, *Phys. Status Solidi* **42**, 559 (1970).
- [5] Klein, U. Microscopic calculations on the vortex state of type II superconductors, *J. Low Temp. Phys.* **69**, 1

- (1987).
- [6] Moshchalkov, V. *et al.* Type-1.5 Superconductivity. *Phys. Rev. Lett.* **102**, 117001 (2009).
- [7] Babaev, E. & Speight, M. Semi-Meissner state and neither type-I nor type-II superconductivity in multicomponent superconductors. *Phys. Rev. B* **72**, 180502(R) (2005).
- [8] Matthias, B. T. *et al.* Superconductivity and Antiferromagnetism in Boron-Rich Lattices. *Science* **159**, 530 (1968).
- [9] Chu, C. *et al.* Boron Isotope Effect in Superconducting Zirconium Dodecaboride. *Science* **159**, 1227 (1968).
- [10] Tsindlekht, M. I. *et al.* Tunneling and magnetic characteristics of superconducting ZrB<sub>12</sub> single crystals. *Phys. Rev. B* **9**, 212508 (2004).
- [11] Khasanov, R. *et al.* Anomalous electron-phonon coupling probed on the surface of superconductor ZrB<sub>12</sub>. *Phys. Rev. B* **72**, 224509 (2005).
- [12] Daghero, D. *et al.* Andreev-reflection spectroscopy in ZrB<sub>12</sub> single crystals. *Supercond. Sci. Technol.* **17**, 8250 (2004).
- [13] Gasparov, V. A. *et al.* Two-gap superconductivity in ZrB<sub>12</sub>: Temperature dependence of critical magnetic fields in single crystals. *Phys. Rev. B* **73**, 094510 (2006).
- [14] Gasparov, V. A. *et al.* 6th Biennial International Workshop on Fullerenes and Atomic Clusters, St. Petersburg (2003); 10th International Workshop on Oxide Electronics, Augsburg (2003).
- [15] Christen D. K. , Kerchner H. R., Sekula S. T. & Thorel P., Equilibrium properties of the fluxoid lattice in single-crystal niobium. II. Small-angle neutron-diffraction measurements. *Phys. Rev. B* **21**, 102 (1980).
- [16] Laver M. *et al.* Structure and degeneracy of vortex lattice domains in pure superconducting niobium: A small-angle neutron scattering study, *Phys. Rev. B* **79**, 014518 (2009).
- [17] Sluchanko, N. *et al.* <sup>10</sup>B<sup>11</sup>B isotope substitution and superconductivity in ZrB<sub>12</sub>. *JETP Letts.* **94**, 642 (2011).
- [18] Gasparov, V. A. *et al.* The de Haasvan Alphen effect study of the Fermi surface of ZrB<sub>12</sub>. *J. Phys.: Conf. Ser.* **150** 052059 (2009).
- [19] Wang, Y. *et al.* Specific heat and magnetization of a ZrB<sub>12</sub> single crystal: Characterization of a type-II/I superconductor. *Phys. Rev. B* **72**, 024548 (2005).
- [20] Sonier, J. E., Brewer, J. H. & Kiefl, R. F.,  $\mu$ SR studies of the vortex state in type-II superconductors. *Rev. Mod. Phys.* **72**, 769 (2000).
- [21] Morenzoni, E, Prokscha, T, Suter, A, Luetkens, H, Khasanov, R, Nano-scale thin film investigations with slow polarized muons, *J. Phys.: Cond. Matt.* **16**, S4583 (2004).
- [22] M. Gladisch, D. Herlach, H. Metz, H. Orth, G. zu Putlitz, A. Seeger, H. Teichler, W. Wahl, and W. Wigand, *Hyperfine Interact.* **6**, 109 (1979).
- [23] Grebinnik V. G. , *et al.* Investigation of superconductors by the muon technique, *Sov. Phys. JETP* **52**, 261 (1980).
- [24] Egorov V. S., Solt G., Baines C., Herlach D., and Zimmermann U., Superconducting intermediate state of white tin studied by muon-spin-rotation spectroscopy, *Phys. Rev. B* **64**, 024524 (2001).
- [25] R. Khasanov, M.M. Radonjić, H. Luetkens, E. Morenzoni, G. Simutis, S. Schönecker, W.H. Appelt, A. Östlin, L. Chioncel, and A. Amato, arXiv:1902.09409 (2019).
- [26] D. Singh, A. D. Hillier, and R. P. Singh, *Phys. Rev. B* **99**, 134509 (2019).
- [27] J. Beare, M. Nugent, M. N. Wilson, Y. Cai, T. J. S. Munsie, A. Amon, A. Leithe-Jasper, Z. Gong, S. L. Guo, Z. Guguchia, Y. Grin, Y. J. Uemura, E. Svanidze, and G. M. Luke *Phys. Rev. B* **99**, 134510 (2019).
- [28] [www.isis.stfc.ac.uk/instruments/musr/](http://www.isis.stfc.ac.uk/instruments/musr/).
- [29] Rainford, B. D. & Daniell, G. J.  $\mu$ SR frequency spectra using the maximum entropy method. *Hyperfine Interact.* **87**, 1129 (1994).
- [30] Kubo R. & Toyabe, T. *Magnetic Resonance and Relaxation. edited by R. Blinc* (North-Holland, Amsterdam, 1967) p. 810.
- [31] Brandt, E. H. & Das, M. Attractive vortex interaction and the intermediate-mixed state of superconductors. *J. Supercond. Novel Magnetism* **24**, 57 (2011).
- [32] Nishio, T. *et al.* Scanning SQUID microscopy of vortex clusters in multiband superconductors. *Phys. Rev. B* **81**, 020506(R) (2010).
- [33] Babaev, E. *et al.* Type-1.5 Superconducting State from an Intrinsic Proximity Effect in Two-Band Superconductors. *Phys. Rev. Lett.* **105**, 067003 (2010).
- [34] Grigorishin, K. V. Effective Ginzburg-Landau free energy functional for multi-band isotropic superconductors. *Phys. Lett. A* **380**, 1781 (2016).
- [35] Riseman, T. *et al.* Observation of a square flux-line lattice in the unconventional superconductor Sr<sub>2</sub>RuO<sub>4</sub>. *Nature* **396**, 242 (1998).
- [36] Yethiraj, M. *et al.* Flux Lattice Symmetry in V<sub>3</sub>Si: Non-local Effects in a High- $\kappa$  Superconductor. *Phys. Rev. Lett.* **82**, 5112 (1999).
- [37] Paul, D. M<sup>c</sup>K. *et al.* Nonlocal Effects and Vortex Lattice Transitions in YNi<sub>2</sub>B<sub>2</sub>C. *Phys. Rev. Lett.* **80**, 1517 (1998).
- [38] Balakrishnan, G., Lees, M. R. & Paul, D. M. Growth of large single crystals of rare earth hexaborides. *J. Crystal Growth* **256**, 206209 (2003).